Research Article

A Method for Aileron Actuator Fault Diagnosis Based on PCA and PGC-SVM

Wei-Li Qin,[1] Wen-Jin Zhang,[1] and Chen Lu[2]

[1]*School of Reliability and Systems Engineering, Beihang University, Beijing 100191, China*
[2]*Science & Technology on Reliability & Environmental Engineering Laboratory, Beijing 100191, China*

Correspondence should be addressed to Chen Lu; luchen@buaa.edu.cn

Aileron actuators are pivotal components for aircraft flight control system. Thus, the fault diagnosis of aileron actuators is vital in the enhancement of the reliability and fault tolerant capability. This paper presents an aileron actuator fault diagnosis approach combining principal component analysis (PCA), grid search (GS), 10-fold cross validation (CV), and one-versus-one support vector machine (SVM). This method is referred to as PGC-SVM and utilizes the direct drive valve input, force motor current, and displacement feedback signal to realize fault detection and location. First, several common faults of aileron actuators, which include force motor coil break, sensor coil break, cylinder leakage, and amplifier gain reduction, are extracted from the fault quadrantal diagram; the corresponding fault mechanisms are analyzed. Second, the data feature extraction is performed with dimension reduction using PCA. Finally, the GS and CV algorithms are employed to train a one-versus-one SVM for fault classification, thus obtaining the optimal model parameters and assuring the generalization of the trained SVM, respectively. To verify the effectiveness of the proposed approach, four types of faults are introduced into the simulation model established by AMESim and Simulink. The results demonstrate its desirable diagnostic performance which outperforms that of the traditional SVM by comparison.

1. Introduction

The aileron actuator, which is used to control the aircraft's rolling movement, is a pivotal component for the flight control system of aircraft [1]. The faults of aileron actuator, which include force motor coil break, sensor coil break, actuator cylinder leakage, and amplifier gain reduction, may cause a series of consequences from control system performance degradation to irretrievable economic loss and personal casualties. Therefore, it is utmost important to research on the fault detection of aileron actuators.

Many fault diagnosis approaches have been used and proposed for classification of system health monitoring data, such as decision tree induction, Bayesian-based classification, neural networks, genetic algorithms, and fuzzy set classifiers [2]. Zhao and Su [3] proposed a novel fault diagnosis method for power transformer insulation based on a decision tree. Ozev et al. [4] presented a parametric fault diagnosis approach for analog/RF circuits based on a Bayesian framework. Zang and Imregun [5] performed structural damage

detection via artificial neural networks. He et al. [6] used immune genetic algorithm to build a mathematical model for fault diagnosis of a modern power system. Altunok et al. [7] presented a damage pattern recognition approach based on fuzzy set theory. However, most of these methods are computationally expensive and their classification accuracy is highly depending on the sample size. Besides, with these methods, some faults such as hydraulic pump fault and external leakage fault can hardly be diagnosed.

Model-based fault detection and diagnosis (FDD) scheme is another important way for FDD of aileron actuators. Henry et al. [8] built an aileron servo-loop model and presented an H_-/H_∞-based solution fitted with the structure of AIRBUS in-service monitoring systems. Vanek et al. [9] founded a reliable linear parameter-varying (LPV) model of the aircraft and performed two inherently different fault detection and isolation designs for aileron and elevator. Gheorghe et al. [10] presented a simple model-based approach for fault detection in both runaway case and jamming case and yielded a more than good performance under real flight test. Goupil and
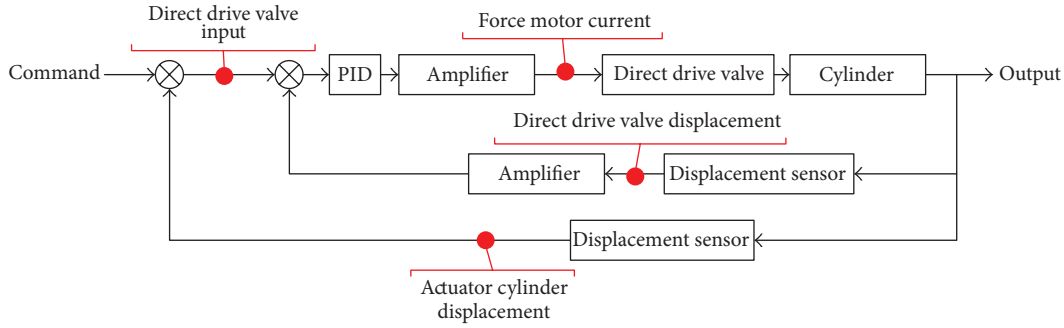
Figure 1: Closed-loop control system of aileron actuator.

Marcos [11] built a generic aircraft model and representative fault scenarios and threw light upon both traditional and advanced model-based FDD approaches. Efimov et al. [12] presented a hybrid observer solution associated with the in-service A380 decision-making rules to solve oscillatory failure case in aircraft system.

Support vector machines (SVMs) which were originally introduced by Vapnik have been successful for solving classification and function estimation problems. Characterized by convex optimization problems (typically quadratic programming), SVM models are capable of obtaining global minimum, avoiding the trap of local minimum brought by the greedy algorithm in other methods. And the ultimate decision function of SVM is determined by, instead of the whole sample, a few support vectors so that computational complexity is reduced and the curse of dimensionality is shunned. Besides, SVM has the advantage of dealing with nonlinear systems while aileron actuator happens to be a typical nonlinear system. SVM is a classical binary classifier and in order to solve multiclassification problem, which is common in fault diagnosis since there are generally more than two failure modes, many SVM algorithms are proposed to construct the multiclassification classifiers. The algorithms adopted in actual application can be divided into two types [13]: (1) the first type is one-time solution method; (2) combining many binary SVM subclassifiers to achieve multiclassification SVM, the second type includes one-versus-rest, one-versus-one, DDAGSVM, and binary-tree SVM. The research related shows that one-versus-one SVM can be more suitable to actual application because of its comparatively fast training speed and good classification accuracy [13–16].

This paper adopts multiclassification algorithm of one-versus-one SVM to design the classifier for the aileron actuator fault diagnosis. In addition, the paper uses grid search to optimize two important parameters C and γ of one-versus-one SVM and Principle Component Analysis (PCA) to reduce dimension. In traditional SVM, the following procedures are usually used: (1) transform data to the format of SVM package; (2) randomly try a few kernels and parameters; (3) test the model. Due to the poor parameter selection and original data complexity, the classification accuracy is relatively unsatisfactory and the training speed is sometimes intolerable. However, the biggest problem is that there will be unclassifiable regions in traditional SVM. The one-versus-one SVM manages to avoid this problem and, with the help

of PCA and grid search, the data complexity and parameter selection problems are solved. Hence, compared to the traditional SVM, the method proposed, through case study, yields a higher classification accuracy and a faster training speed while external leakage fault can be effectively diagnosed by the method. Generally, the most important thing to do in aeronautical engineering is to perform an early fault detection to switch as soon as possible on a redundant actuator. Once properly trained on ground using historical data, the proposed algorithm can achieve fault classification as fast as 0.1∼ 1 s each time. With the development Flight Control Computer (FCC), its constraints such as low computational load and restricted symbol library will not be a problem for relatively complex algorithms in the future. On that basis, high fault classification accuracy will be a bonus since corresponding maintenance preparation can be done before the landing of the aircraft and thus efficiency is improved.

The remainder of the paper is organized as follows. In Section 2, a joint simulation model of aileron actuator based on AMESim and Simulink is set up. In Section 3, the faults of aileron actuator are analyzed and injected into the model. In Section 4, a detailed description of the proposed method is presented. In Section 5, the effectiveness of the proposed approach is demonstrated and the results of experimental are presented and discussed. Finally, the conclusion of the research will be given.

2. Setup of Aileron Actuator

The aileron actuator consists of a hydraulic pump, an electro-hydraulic servo valve, a cylinder, a PID controller, two electronic amplifiers, and two displacement sensors. The control loop includes two position feedbacks—direct drive valve displacement and actuator cylinder displacement, as is shown in Figure 1. In this figure, the signals used for fault detection are marked with red ball.

The simulation model of the aileron actuator is established with MATLAB Simulink and AMESim [17]. Simulink, developed by MathWorks, is the visual simulation environment in MATLAB. Thanks to its convenient graphic model modules such as linear/nonlinear modules, continuous/discrete modules, and advanced control toolboxes, it is quite fit for control loop modeling. However, it could not handle hydraulic modeling lacking corresponding modules. AMESim, developed by Imagine, is a hydraulic/mechanical
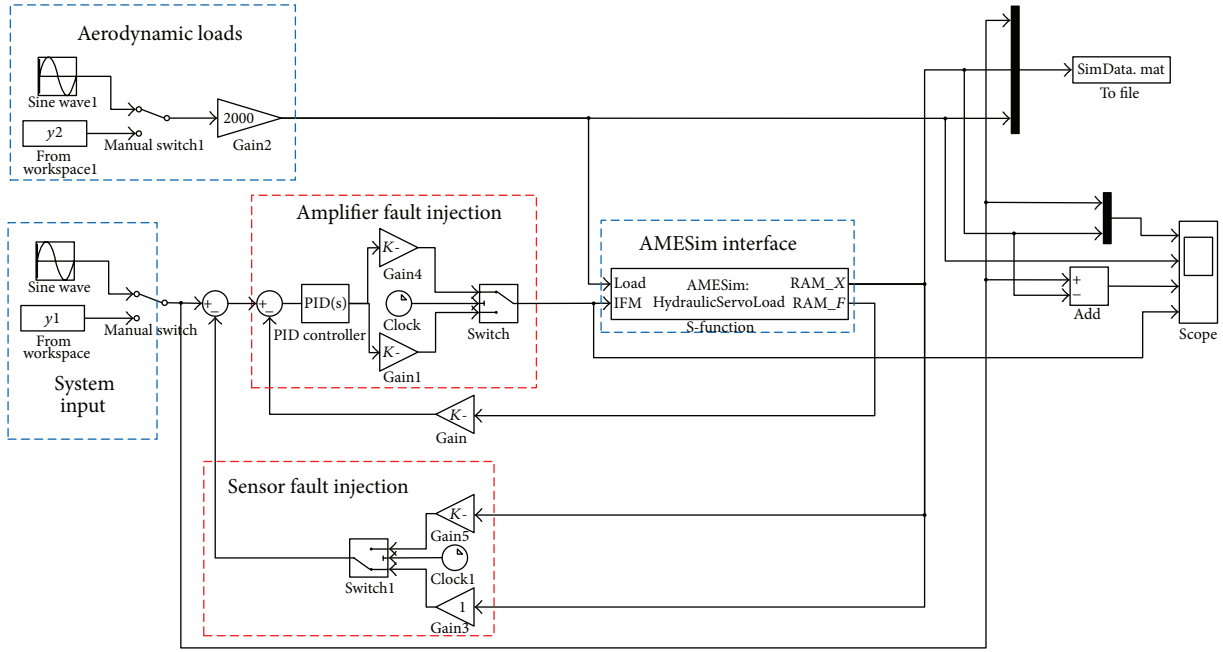
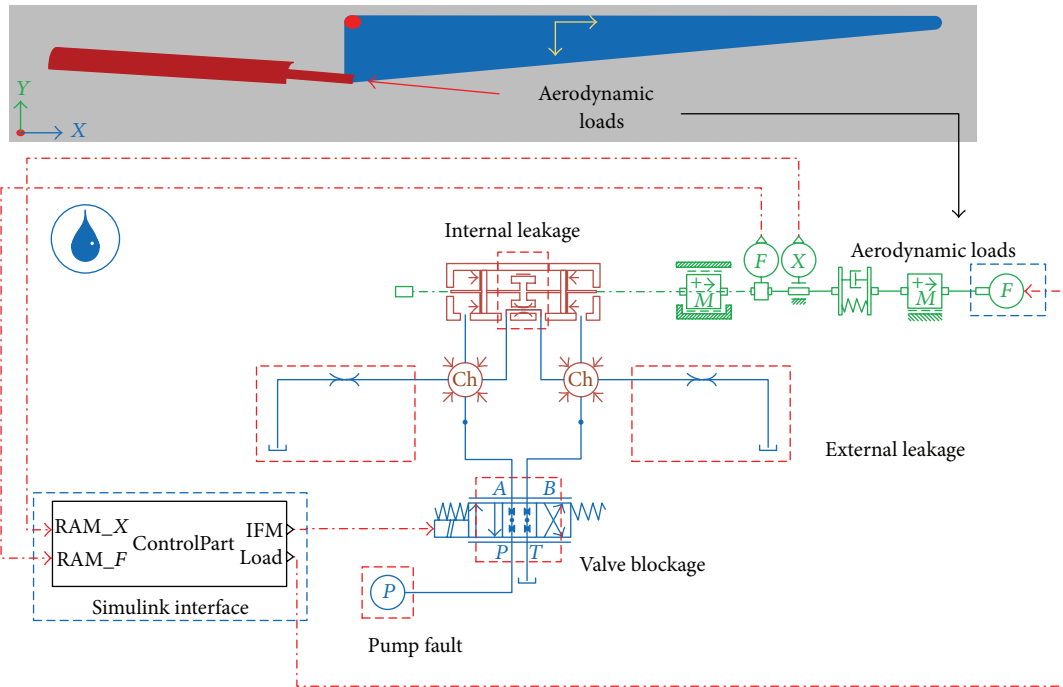Figure 2: Control part of aileron actuator in Simulink.

Figure 3: Mechanical part of aileron actuator in AMESim.

system modeling, simulation, and analysis software. With abundant parameterized hydraulic modules, the hydraulic part of the aileron actuator can be easily founded. However, there are relatively few control modules in AMESim. With the combination of Simulink and AMESim, the advantages of these two can be fully utilized and thereby a relatively good model of aileron actuator is promising. The control part of the aileron actuator established in Simulink environment is shown in Figure 2; the mechanical part of the aileron actuator is shown in Figure 3. The mechanical part of the aileron actuator established in AMESim is converted to a Simulink S-Function, and the S-Function can be imported to Simulink. The physical parameters of the key components are described in Tables 1–9.

TABLE 1: Elementary hydraulic properties.

FP04-1: all real parameters	Unit	Value
Density	kg/m^3	850
Bulk modulus	Bar	17000
Slope of bulk modulus [bar] in function of pressure [bar] (in percentage)	Null	0
Absolute viscosity	cP	51
Absolute viscosity of air/gas	cP	0.02
Saturation pressure (for dissolved air/gas)	Bar	0
Air/gas content	%	0.1
Temperature	degC	40
Temperature $T1$	degC	40
Kinematic viscosity at ($Patm$, $T1$)	cSt	56.47
Temperature $T2$	degC	100
Kinematic viscosity at ($Patm$, $T2$)	cSt	9.71
Coefficient for temperature viscosity characteristic	Null	200
Polytropic index for air/gas/vapor content	Null	1.4
(Advanced user) High saturated vapor pressure	Bar	−0.5
(Advanced user) Low saturated vapor pressure	Bar	−0.6
(Advanced user) Absolute viscosity of vapor	cP	0.02
(Advanced user) Effective molecular mass of vapor	Null	200
(Advanced user) Air/gas density at atmospheric pressure 0 degC	kg/m^3	1.2

TABLE 2: Parameters of pressure source.

PS00-1: all real parameters	Unit	Value
Time at which duty cycle starts	s	0
Pressure at start of stage 1	Bar	210
Pressure at end of stage 1	Bar	210
Duration of stage 1	s	$1e + 06$

One leakage/viscous friction module, which is utilized for cylinder internal leakage fault injection [18], and two piston modules constitute the simulation model of the hydraulic cylinder of the aileron actuator.

In this paper, the aileron actuator works at normal temperature, 40°C, which is shown, as a part of elementary hydraulic properties, in Table 1. And the kinematic viscosity will decrease when temperature increases.

Under normal condition, the pressure of the pump as shown in Table 2 is 210 bar.

Under normal condition, the pressure drops and the flow rate at maximum valve opening as shown in Table 3 is 20 bar and 150 L/min.

Under normal condition, the clearance diameter as shown in Table 4 is set to $1e − 05$ mm. And it will be increased in order to inject the internal leakage fault.

The chamber length at zero displacement, the rod diameter, and the piston diameter as shown in Table 5 are 150 mm, 30 mm, and 90 mm.

The gain for signal output as shown in Table 6 is set to be 1.

The mass and displacement module, whose parameters are shown in Table 7, is adopted to confine the hydraulic cylinder's movement scope.

The spring damper, whose parameters are shown in Table 8, is adopted for simulation of the damp of aerodynamic loads.

In Table 9, list the parameters of flow control valve.

3. Fault Analysis and Injection

According to statistical maintenance data, main faults of an aileron actuator include amplifier fault, sensor fault, leakage fault, external leakage fault, pump fault, and valve fault, which are listed in Table 10.

Failure mode, effects, and criticality analysis (FMECA) is a bottom-up, inductive analytical method for fault analysis. According to the FMECAs of hydraulic system made by Li et al. [19] and Balaban et al. [20], these faults can be roughly divided into four quadrants depending on their criticality and frequency. As shown in Figure 4, the first-quadrant faults are high-frequency and high-criticality so that normally they have to be considered in design phase. The second-quadrant faults, currently dealing with visual inspection, are high-frequency but low-criticality. The third-quadrant faults are low-frequency and low-criticality and thus are dismissed taking cost into consideration. The fourth-quadrant faults, which need constant monitoring, are low-frequency but high-criticality.

To demonstrate the approach presented in this paper, four faults including electronic faults and mechanical faults were introduced into the simulation model and listed in Table 11.

The faults listed in Tables 10 and 11 were introduced into the simulation model by changing several specific parameters of the fault component, and these components were marked with red box in Figures 2 and 3. The details of fault injection were listed in Table 12. The parameter of force motor fault

Table 3: Parameters of servo valve.

SV00-1: all real parameters	Unit	Value
Ports P to A flow rate at maximum valve opening	L/min	150
Ports P to A corresponding pressure drop	Bar	20
Ports P to A critical flow number (laminar $\rightarrow$ turbulent)	Null	1000
Ports B to T flow rate at maximum valve opening	L/min	150
Ports B to T corresponding pressure drop	Bar	20
Ports B to T critical flow number (laminar $\rightarrow$ turbulent)	Null	1000
Ports P to B flow rate at maximum valve opening	L/min	150
Ports P to B corresponding pressure drop	Bar	20
Ports P to B critical flow number (laminar $\rightarrow$ turbulent)	Null	1000
Ports A to T flow rate at maximum valve opening	L/min	150
Ports A to T corresponding pressure drop	Bar	20
Ports A to T critical flow number (laminar $\rightarrow$ turbulent)	Null	1000
Working density for pressure drop measurement	kg/m^3	850
Working kinematic viscosity for pressure drop measurement	cSt	60
Valve rated current	mA	1
Valve natural frequency	Hz	500
Valve damping ratio	Null	0.8
Deadband as fraction of spool travel	Null	0

Table 4: Parameters of leakage and viscous friction module.

BAF11-1: all real parameters	Unit	Value
External piston diameter	mm	90
Clearance on diameter	mm	$1e-05$
Length of contact	mm	30

Table 5: Parameters of piston modules.

BAP11-1: all real parameters	Unit	Value
Piston diameter	mm	90
Rod diameter	mm	30
Chamber length at zero displacement	mm	150

Table 6: Parameters of displacement sensor.

DT000-1: all real parameters	Unit	Value
Offset to be subtracted from displacement	M	0
Gain for signal output	1/m	1

Table 7: Parameters of mass and displacement module.

MAS005-1: all real parameters	Unit	Value
Mass	kg	10
Coefficient of viscous friction	N/(m/s)	5000
Coefficient of windage	N/(m/s)^2	0
Coulomb friction force	N	1000
Stiction force	N	1000
Lower displacement limit	m	−0.15
Higher displacement limit	m	0.15
Inclination (+90 port 1 lowest, −90 port 1 highest)	Degree	0

Table 8: Parameters of spring damper.

SD000-1: all real parameters	Unit	Value
Spring rate	N/m	$1e+06$
Displacement giving zero spring force	m	0
Damper rating	N/(m/s)	10000

Table 9: Parameters of flow control valve.

OR0000: all real parameters	Unit	Value
Characteristic flow rate	L/min	1
Corresponding pressure drop	bar	1
Equivalent orifice diameter	mm	$1e-05$
Maximum flow coefficient	null	0.7
Critical flow number (laminar $\rightarrow$ turbulent)	Null	1000

is set to 0, indicating force motor coil break; the parameter of sensor fault is set to 0, indicating sensor coil break; the parameter of leakage fault is set to 5 instead of the default normal value $1e-5$, indicating 5.56% leakage since the diameter of the valve is 90 mm; the parameter of amplifier fault is set to 15 instead of the default normal value 50, indicating 70% signal transmitting loss. All the faults were introduced into the simulation model in advance of stimulation.

4. Methodology

The proposed method in the paper consists of two major parts, the model training using historical data and the real-time diagnosis using real-time data. In model training part,

TABLE 10: Fault analysis of aileron actuator.

Object	Fault mode	Fault cause	Fault phenomenon
Direct driving valve	Force motor coil shutoff	Force motor coil break	Force motor has no power output; the position of valve element is constantly in the neutral position.
	Blockage	Oil pollution	Null bias increases; frequency response decreases; system is unstable.
	Valve element stuck	Oil pollution Slide valve distortion	The direct driving valve output constant flow; the system pressure decreases.
	Valve leakage	Edge abrasion Radial valve element abrasion	Null bias increases; gain of system decreases; system pressure decreases; flow noise increases.
	Null bias out-of-tolerance	Inaccurate zero setting	Bias exists when DDV is at null position.
Displacement sensor	Coil break	Cable break	Sensor has no output.
	Constant bias	Iron core of sensor loose	Displacement bias.
Actuator cylinder	External leakage	Sealing washers fail Hydraulic leakage	The speed of moving parts decreases; system pressure decreases.
	Internal leakage out-of- tolerance	Cylinder abrasion Oil in high pressure area flow into low pressure area	The speed of moving parts decreases; system pressure decreases; vibration and noise appear.
Electronic amplifier	Gain reduction	Internal faults of electronic amplifier	Magnification notably decreases.

TABLE 11: Fault mode and details.

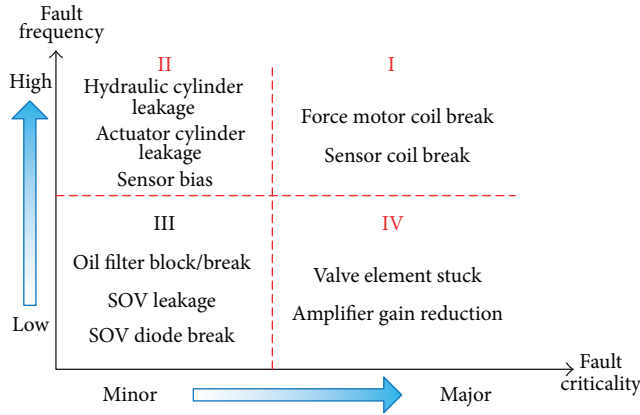| Number	Fault mode	Fault type	Details	Quadrant
1	Force motor fault	Mechanical fault	Force motor coil break	I
2	Sensor fault	Electronic fault	Sensor coil break	I
3	Leakage fault	Mechanical fault	Actuator cylinder leakage run out of tolerance	II
4	Amplifier fault	Electronic fault	Amplifier gain reduction	IV

FIGURE 4: Aileron actuator fault quadrantal diagram.

three steps are conducted. Firstly, historical data which include DDV input, force motor current, DDV displacement, and actuator cylinder displacement are corrupted by white noise with signal-noise ratio to be 20 dB in MATLAB. Then, the corrupted data are truncated into a number of data segments according to the data period. And the mean, root mean square (RMS), peak-to-peak value (ppV), and kurtosis of these data segments are calculated and normalized, respectively. Hence 16-dimensional primitive inputs, shown in Table 13, are obtained. It is worth mentioning that the dimensions of the primitive inputs are not specially chosen since the key fault information will be automatically extracted by PCA. The flow chart of first step is shown in Figure 5. Secondly, PCA is utilized to conduct dimension reduction and noise reduction and thus the reduced inputs for the SVM model are got. Thirdly, the reduced inputs are input to the SVM model for parameter optimization using grid search. Once the optimal parameters for the SVM model are searched, the trained model is prepared for the real-time diagnosis. In Real-time diagnosis, real-time data are acquired by sensors deployed on the air craft. The same data preprocess as in model training part is conducted and the classification result is returned by the trained SVM model. Fault report would be generated for the pilot or ground control station if the classification results meet a certain fault criterion. The flow chart of the method is shown in Figure 6.

4.1. PCA. Invented by Karl Pearson, PCA adopts orthogonal mapping to map a set of possibly correlated variables to principal components that are linearly uncorrelated. The greatest variance lies on the first principal component, the second greatest variance on the second principal component, and so on.

TABLE 12: Fault injection details.

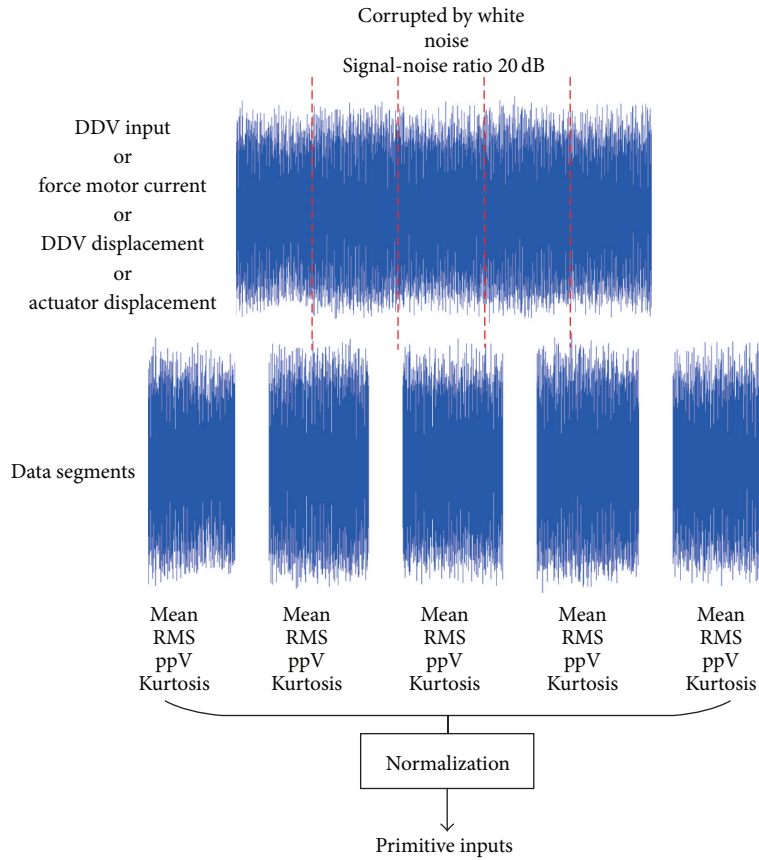| Test number	Fault mode	Fault component	Changed parameter for fault injection (unit)	Parameter (normal)	Parameter (fault)
1	Force motor fault	Force motor	FMC gain	1	0
2	Sensor fault	Displacement sensor	Signal output (1/m)	1	0
3	Leakage fault	Actuator cylinder	Flow control valve equivalent orifice diameter (mm)	$1e-5$	5
4	Amplifier fault	Electronic amplifier	Gain	50	15

FIGURE 5: Flow chart of data preprocess.

Here is a data matrix, X, whose n rows are n different repetition of the experiment and whose p columns are p different parameters: $X = (X_{(1)}, \ldots, X_{(i)}, \ldots, X_{(n)})^T$, $X_{(i)} = (x_1, \ldots, x_p)_{(i)}$. The scores of new vector of principal components $\mathbf{t}_{(i)} = (t_1, \ldots, t_p)_{(i)}$, $i = 1, 2, \ldots, n$, where i is ordinal number of the row, are given through a mathematical transformation defined by p-dimensional vectors of weights $\mathbf{w}_{(k)} = (w_1, \ldots, w_p)^T_{(k)}$, $k = 1, 2, \ldots, p$, where k is the ordinal number of the principal component. The equation is shown as below:

$$t_{k(i)} = \mathbf{X}_{(i)} \cdot \mathbf{w}_{(k)}, \tag{1}$$

where $t_{k(i)}$ is the kth component of $X_{(i)}$, and thus the maximum possible variance from X is inherited by $\mathbf{t}$ with each vector of weight $\mathbf{w}$ constrained as a unit vector.

The first component of a data vector $\mathbf{X}_{(i)}$ can then be given as a score $t_{1(i)} = \mathbf{X}_{(i)} \cdot \mathbf{w}_{(1)}$ in the transformed coordinates, where $\mathbf{w}_{(1)}$ has to satisfy

$$\mathbf{w}_{(1)} = \underset{\|\mathbf{w}\|=1}{\operatorname{argmax}} \left\{ \sum_i (t_1)^2_{(i)} \right\} = \underset{\|\mathbf{w}\|=1}{\operatorname{argmax}} \left\{ \|\mathbf{X}\mathbf{w}\|^2 \right\}$$
$$= \underset{\|\mathbf{w}\|=1}{\operatorname{argmax}} \left\{ \mathbf{w}^T \mathbf{X}^T \mathbf{X} \mathbf{w} \right\}, \tag{2}$$
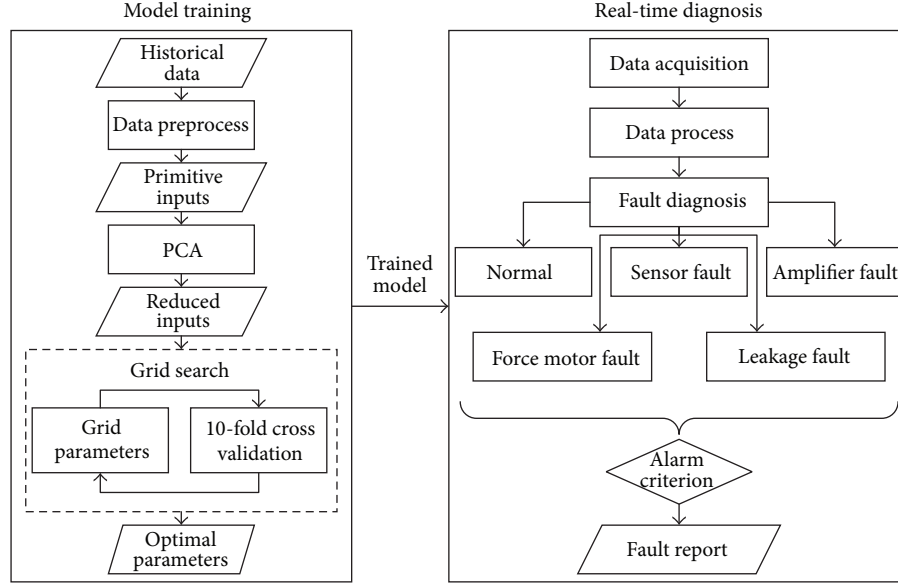
FIGURE 6: Flow chart of fault diagnosis.

TABLE 13: Primitive inputs for SVM model.

Model input	Features	Object
Input 1		Direct drive valve input
Input 2	Mean	Force motor current
Input 3		Direct drive valve displacement
Input 4		Actuator cylinder displacement
Input 5		Direct drive valve input
Input 6	RMS	Force motor current
Input 7		Direct drive valve displacement
Input 8		Actuator cylinder displacement
Input 9		Direct drive valve input
Input 10	ppV	Force motor current
Input 11		Direct drive valve displacement
Input 12		Actuator cylinder displacement
Input 13		Direct drive valve input
Input 14	Kurtosis	Force motor current
Input 15		Direct drive valve displacement
Input 16		Actuator cylinder displacement

and the kth component can be found by subtracting the first $k - 1$ principal components from $\mathbf{X}$:

$$\widehat{\mathbf{X}}_k = \mathbf{X} - \sum_{s=1}^{k-1} \mathbf{X}\mathbf{w}_{(s)}\mathbf{w}_{(s)}^T, \tag{3}$$

and then finding the weight vector which extracts the maximum variance from this new data matrix

$$\mathbf{w}_{(k)} = \underset{\|\mathbf{w}\|=1}{\operatorname{argmax}} \left\{ \left\| \widehat{\mathbf{X}}_k\mathbf{w} \right\|^2 \right\} = \underset{\|\mathbf{w}\|=1}{\operatorname{argmax}} \left\{ \mathbf{w}^T\widehat{\mathbf{X}}_k^T\widehat{\mathbf{X}}_k\mathbf{w} \right\}, \tag{4}$$

the kth component of a data vector $\mathbf{X}_{(i)}$ can then be given as a score $t_{k(i)} = \mathbf{X}_{(i)} \cdot \mathbf{w}_{(k)}$ in the transformed coordinates.

The full principal component decomposition of $\mathbf{X}$ can therefore be given as

$$\mathbf{T} = \mathbf{X}\mathbf{W}, \tag{5}$$

where $\mathbf{W}$ is a p-by-p matrix whose columns are the eigenvectors of $\mathbf{X}^T\mathbf{X}$.

4.2. Grid Search and CV. Grid search executes exhaustive searching through an artificially selected parameter set of certain learning algorithms. A typical soft-margin SVM classifier equipped with an RBF kernel has two parameters that need to be tuned: a regularization constant C and a kernel hyper parameter γ. The goal of grid search is to identify good pair (C, γ) so that the classifier can accurately predict unknown data. Exponentially growing sequences of C and γ (e.g., $C = 2^{-5}, 2^{-3}, \ldots, 2^{15}$, $\gamma = 2^{-15}, 2^{-13}, \ldots, 2^3$) are recommended by Hsu et al. [21].

In contrast with other optimization algorithms such as genetic algorithm and particle swarm algorithm, the grid search is straightforward but seems naive. However, there are two motivations why I prefer the simple grid-search approach. One is that, psychologically, we may not feel safe to use methods which avoid doing an exhaustive parameter search by approximations or heuristics. The other reason is that the computational time required to find good parameters by grid search is not much more than that by advanced methods since there are only two parameters in this case. Furthermore, the grid search can be easily parallelized because each (C, γ) is independent. Many of advanced methods are iterative processes, for example, walking along a path, which can be hard to parallelize.

And the performance of the pair is assessed by cross validation on the training set. The training set is divided into

v equal-sized subsets in v-fold cross validation. In proper sequence, each subset is used for test while other $v - 1$ subsets are used for classifier training. Hence, v prediction results are obtained and the percentage of data correctly classified is the final cross validation accuracy. Rodriguez et al. [22] conducted a sensitivity analysis for cross validation and found 10-fold cross validation is a practical method.

4.3. One-versus-One SVM. One-versus-one SVM is proposed by Knerr et al. [23] that transform the n-classification problem into $n(n - 1)/2$ two-classification problem. One-versus-one SVM adopts the voting method to get, respectively, the number of votes that the sample x belongs to each classification. In the end, x belongs to the classification in which the number of votes is the largest. Hsu and Lin [24] compared one-versus-one SVM, one-versus-all SVM, and DAG-SVM and the results showed that one-versus-one SVM may be more suitable for practical use.

In order to construct the subclassifier for class i and j, take the sample of class i and class j from the original sample as the training sample for two-classification problem; the optimal problem is shown as follows:

$$\min_{\omega^{ij}, b^{ij}, \xi^{ij}} \quad \frac{1}{2} \left(\omega^{ij} \right)^T \omega^{ij} + C \sum_{j=1}^{i} \xi_i^{ij} \left(\omega^{ij} \right)^T. \tag{6}$$

Corresponding decisive plane is

$$
\begin{aligned}
\left(\omega^{ij} \right)^T \phi \left(x_t \right) + b^{ij} &\geq 1 - \xi_i^{ij}, \quad \text{if } y_t = i, \\
\left(\omega^{ij} \right)^T \phi \left(x_t \right) + b^{ij} &\leq -1 + \xi_i^{ij}, \quad \text{if } y_t = j, \ \xi_i^{ij} \geq 0,
\end{aligned}
\tag{7}
$$

where ω^{ij} is the coefficient of the hyperplane between classes i and j, b^{ij} is the intercept of the hyperplane between classes i and j, $\phi(x_t)$ is the map of the sample x_t in the high-dimension space, C is error penalty factor which reflects the valued degree of sample outliers and adjusts the proportion between the incredible range and empirical risk of SVM network model, and ξ_i^{ij} is the fitting error variable.

4.4. Alarm Criterion. With the continuous development of FCC, the limitation of FCC will be kept pushing. Once the computational limits were broken and complex algorithm could also achieve practically fast fault detection, then in order to reduce false alarm rate to the greatest extent, three-alarm criterion listed below can be attempted.

Criterion 1 (two consecutive classification results concur). If two consecutive classification results concur, then the classification results are validated and the corresponding fault can be reported.

Criterion 2 (two out of three consecutive classification results concur). If the first two consecutive classification results differ and yet two out of three consecutive classification results concur, then the classification results are validated and the corresponding fault denoted by the two same classification results can be reported.

TABLE 14: Contribution rate of principal component.

Principal component	Eigenvalue	Contribution rate	Cumulative contribution rate
1	4.0114	83.44%	83.44%
2	0.1995	4.15%	87.59%
3	0.1339	2.79%	90.38%
4	0.1257	2.61%	92.99%
5	0.1048	2.18%	95.17%
6–16	<0.1	<2%	>95.17%

TABLE 15: The cross validation rate and test rate with regard to different dimension of inputs.

Dimension	CV rate	Test rate
1	76.73%	76.75%
2	82.08%	83.05%
3	89.37%	89.87%
4	96.63%	96.50%
5	98.88%	99.01%

Criterion 3 (none of three consecutive classification results concur). If three consecutive classification results all differ, then the diagnosis fails and the diagnosis-fail report will be submitted.

5. Fault Diagnosis and Result Analysis

In this simulation case, the amplitude of system input is 2 mm, the frequency of system input is 0.5 Hz, the sampling rate is 200 S/s, and the sampling time is 20 s. Accordingly, the features, which include mean, RMS, ppV, and kurtosis, are extracted every 200 points. The data obtained are considered as the historical data to train the model. Once trained, the model can be used to detect faults every 200 points (less than 1 s depending on the real-time sampling rate) in real-time diagnosis. The extracted features at different working conditions are listed in Figure 7, from which it is clear to see that different working conditions result in different feature amplitude so that fault classification using these features is positively tenable.

The results of PCA for the 16-dimensional primitive inputs are shown in Table 14 and Figure 8, from which it is clear to see that the first three principal components occupy up to 100% cumulative contribution rate and that the inputs dimension may even be reduced to just 1-dimension depending on the ultimate test rate of the trained model.

As shown in Table 15, using just the first principal component to train the model, the trained model's cross validation rate is 76.73% and test rate is 76.75%, which implies overreduction and information loss. Using first five principal components to train the model, the trained model's cross validation rate is increased up to 98.88% and test rate to 99.01%, close to 1, which is more than good so the reduced inputs can be determined as three-dimensional.
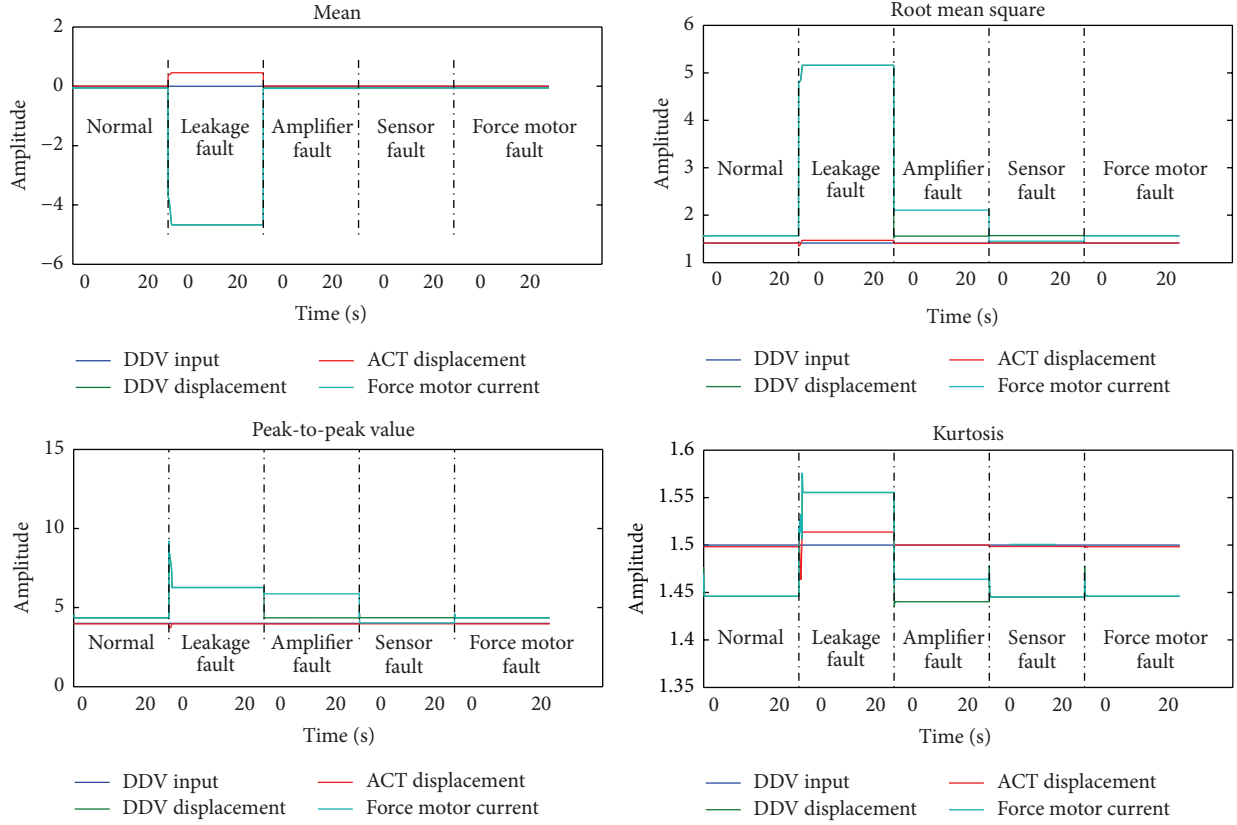
FIGURE 7: Features extracted.

TABLE 16: Comparison between traditional SVM and PGC-SVM.

Method	Time cost		Classification accuracy
	Parameters optimization	Training	
General SVM	days even months	1.5884 s	81.87%
PGC-SVM	8 h 20 mins	0.8989 s	98.88%

There are two parameters, penalty factor C and kernel parameter γ, to be optimized in one-versus-one SVM using RBF kernel which is shown below:

$$K\left(x, x'\right) = \exp\left(\gamma \left\|x - x'\right\|^2\right). \tag{8}$$

The exponentially growing sequences of parameter pairs (C, γ) are adopted in grid search and the contour of parameter pairs is shown in Figure 9. The best pair $(C = 4096, \gamma = 1)$, whose cross validation accuracy was up to 98.87%, was obtained.

The final results, shown in Table 16, indicated that the PGC-SVM proposed in the paper outperformed traditional SVM in both time cost (Pentium(R) Dual-Core CPU T4500 @ 2.30 GHz) and classification accuracy.

6. Conclusions

This paper presents an aileron actuator fault diagnosis approach combining principal component analysis (PCA),
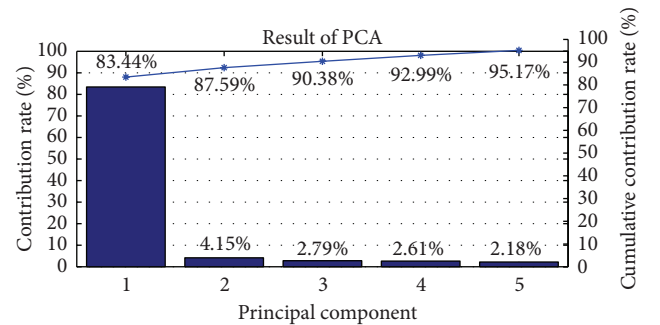

FIGURE 8: Result of PCA.

grid search (GS), 10-fold cross validation (CV), and one-versus-one support vector machine (SVM). The classification accuracy is good enough for the diagnosis of the main faults of aileron actuators which include force motor coil break, sensor coil break, actuator cylinder leakage, and amplifier gain

Best $\log2(C) = 12$, $\log2(\gamma) = 0$, accuracy = 98.87%,
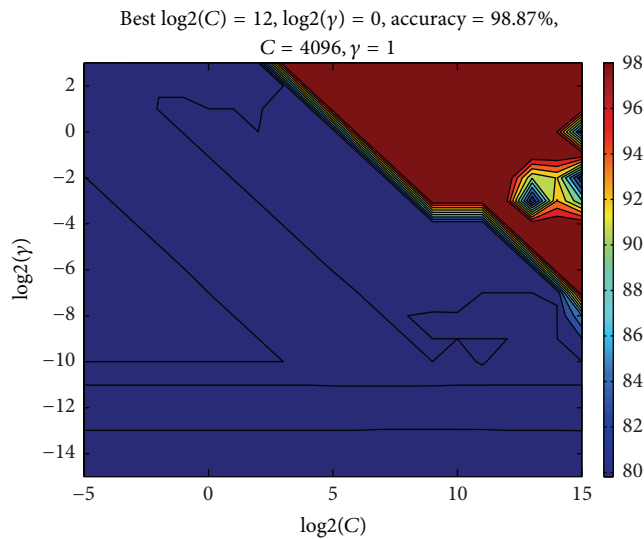$C = 4096$, $\gamma = 1$

FIGURE 9: Grid search for model with PCA.

reduction. Compared to the traditional SVM, the PGC-SVM demands less time for both parameters optimization and model training. The performance of the proposed algorithm is fast enough for fault detection to switch as soon as possible on a redundant actuator. The high classification accuracy of actuator faults gives the algorithm a bonus that maintenance efficiency can be promoted since maintenance preparation can be done before the landing of aircraft. Hence, the algorithm presented in the paper shows a great potential once it passed the rigorous test of real FCC.

Obviously, the future work lies in the field validation of the proposed algorithm. And in practice, the field data are often severely corrupted by various data noise that may influence the performance of the algorithm so that noise immunity of the proposed algorithm should also be considered. Besides, the method still has some room for improvement—the computational resource consumption can be compressed further and detection delay can be minimized.

Conflict of Interests

The authors declare that there is no conflict of interests regarding the publication of this paper.

Authors' Contribution

Wei-Li Qin and Chen Lu drafted the paper; Wei-Li Qin and Chen Lu acquired the data; Wei-Li Qin analyzed and interpreted the data; Wei-Li Qin and Chen Lu critically revised the paper; Chen Lu and Wen-Jin Zhang planned and supervised the research.

Acknowledgments

References

[1] Y. Chinniah, R. Burton, S. Habibi, and E. Sampson, "Identification of the nonlinear friction characteristics in a hydraulic actuator using the extended Kalman filter," *Transactions of the Canadian Society for Mechanical Engineering*, vol. 32, no. 2, pp. 121–136, 2008.

[2] I. Lopez and N. Sarigul-Klijn, "A review of uncertainty in flight vehicle structural damage monitoring, diagnosis and control: challenges and opportunities," *Progress in Aerospace Sciences*, vol. 46, no. 7, pp. 247–273, 2010.

[3] F. Zhao and H. Su, "A decision tree approach for power transformer insulation fault diagnosis," in *Proceedings of the 7th World Congress on Intelligent Control and Automation (WCICA '08)*, pp. 6882–6886, IEEE, Chongqing, China, June 2008.

[4] S. Ozev, P. K. Nikolov, and F. Liu, "Parametric fault diagnosis for analog circuits using a bayesian framework," in *Proceedings of the 24th IEEE VLSI Test Symposium IEEE Computer Society*, pp. 272–277, Berkeley, Calif, USA, May 2006.

[5] C. Zang and M. Imregun, "Structural damage detection using artificial neural networks and measured FRF data reduced via principal component projection," *Journal of Sound and Vibration*, vol. 242, no. 5, pp. 813–827, 2001.

[6] L. He, K.-N. Jia, and Z.-Q. Fan, "The immune genetic algorithm in fault diagnosis of modern power system," in *Proceedings of the 2nd International Conference on Education Technology and Computer (ICETC '10)*, vol. 4, pp. V4-26–V4-29, IEEE, Shanghai, China, June 2010.

[7] E. Altunok, M. M. R. Taha, D. S. Epp, R. L. Mayes, and T. J. Baca, "Damage pattern recognition for structural health monitoring using fuzzy similarity prescription," *Computer-Aided Civil & Infrastructure Engineering*, vol. 21, no. 8, pp. 549–560, 2006.

[8] D. Henry, J. Cieslak, A. Zolghadri, and D. Efimov, "A non-conservative H_-/H_∞ solution for early and robust fault diagnosis in aircraft control surface servo-loops," *Control Engineering Practice*, vol. 31, no. 1, pp. 183–199, 2014.

[9] B. Vanek, A. Edelmayer, Z. Szabó, and J. Bokor, "Bridging the gap between theory and practice in LPV fault detection for flight control actuators," *Control Engineering Practice*, vol. 31, no. 1, pp. 171–182, 2014.

[10] A. Gheorghe, A. Zolghadri, J. Cieslak, P. Goupil, R. Dayre, and H. L. Berre, "Model-based approaches for fast and robust fault detection in an aircraft control surface servo loop from theory to flight tests," *IEEE Control Systems Magazine*, vol. 33, pp. 20–84, 2013.

[11] P. Goupil and A. Marcos, "The European ADDSAFE project: industrial and academic efforts towards advanced fault diagnosis," *Control Engineering Practice*, vol. 31, pp. 109–125, 2014.

[12] D. Efimov, J. Cieslak, A. Zolghadri, and D. Henry, "Actuator fault detection in aircraft systems: oscillatory failure case study," *Annual Reviews in Control*, vol. 37, no. 1, pp. 180–190, 2013.

[13] T. Yaohua, G. Jinghuai, and B. Qianzong, "Novel selective support vector machine ensemble learning algorithm," *Journal of Xi'an Jiaotong University*, vol. 42, no. 10, pp. 1221–1225, 2008.

[14] W. Jiang and S. Wu, "Multi-data fusion fault diagnosis method based on SVM and evidence theory," *Chinese Journal of Scientific Instrument*, vol. 31, no. 8, pp. 1738–1743, 2010.

[15] X. Gu, S. Yang, and S. Qian, "On rotary machine's multi-class fault recognition based on SVM," in *Proceedings of the 26th Chinese Control Conference (CCC '07)*, pp. 460–463, IEEE, Hunan, China, July 2007.

[16] S.-L. Zhao and Y.-C. Zhang, "SVM classifier based fault diagnosis of the satellite attitude control system," in *Proceedings of the International Conference on Intelligent Computation Technology and Automation (ICICTA '08)*, pp. 907–911, Hunan, China, October 2008.

[17] Z. Zhao, M. Jia, F. Wang, and S. Wang, "Intermittent chaos and sliding window symbol sequence statistics-based early fault diagnosis for hydraulic pump on hydraulic tube tester," *Mechanical Systems and Signal Processing*, vol. 23, no. 5, pp. 1573–1585, 2009.

[18] J. Yao, G. Yang, and D. Ma, "Internal leakage fault detection and tolerant control of single-rod hydraulic actuators," *Mathematical Problems in Engineering*, vol. 2014, Article ID 345345, 14 pages, 2014.

[19] P. Li, Z.-H. Yuan, and F. Su, "Reliability analysis of electrohydraulic actuator based on fuzzy FMECA," *Machine Tool & Hydraulics*, vol. 7, pp. 178–182, 2013.

[20] E. Balaban, A. Saxena, P. Bansal, K. F. Goebel, P. Stoelting, and S. Curran, "A diagnostic approach for electro-mechanical actuators in aerospace systems," in *Proceedings of the IEEE Aerospace Conference*, pp. 1–13, IEEE, Big Sky, Mont, USA, March 2009.

[21] C.-W. Hsu, C.-C. Chang, and C.-J. Lin, *A Practical Guide to Support Vector Classification*, Department of Computer Science & Information Engineering National Taiwan University, 2010.

[22] J. D. Rodriguez, A. Perez, and J. A. Lozano, "Sensitivity analysis of k-fold cross validation in prediction error estimation," *IEEE Transactions on Pattern Analysis & Machine Intelligence*, vol. 32, no. 3, pp. 569–575, 2010.

[23] S. Knerr, L. Personnaz, and G. Dreyfus, "Single-layer learning revisited: a stepwise procedure for building and training a neural network," in *Neurocomputing*, pp. 41–50, Springer, 1990.

[24] C.-W. Hsu and C.-J. Lin, "A comparison of methods for multiclass support vector machines," *IEEE Transactions on Neural Networks*, vol. 13, no. 2, pp. 415–425, 2002.